Biophysical Journal Volume 101 October 2011 1921–1929

Effect of Hydroperoxides on Red Blood Cell Membrane Mechanical Properties

John P. Hale, C. Peter Winlove, and Peter G. Petrov*
School of Physics, University of Exeter, Exeter, United Kingdom

ABSTRACT We investigate the effect of oxidative stress on red blood cell membrane mechanical properties in vitro using detailed analysis of the membrane thermal fluctuation spectrum. Two different oxidants, the cytosol-soluble hydrogen peroxide and the membrane-soluble cumene hydroperoxide, are used, and their effects on the membrane bending elastic modulus, surface tension, strength of confinement due to the membrane skeleton, and 2D shear elastic modulus are measured. We find that both oxidants alter significantly the membrane elastic properties, but their effects differ qualitatively and quantitatively. While hydrogen peroxide mainly affects the elasticity of the membrane protein skeleton (increasing the membrane shear modulus), cumene hydroperoxide has an impact on both membrane skeleton and lipid bilayer mechanical properties, as can be seen from the increased values of the shear and bending elastic moduli. The biologically important implication of these results is that the effects of oxidative stress on the biophysical properties, and hence the physiological functions, of the cell membrane depend on the nature of the oxidative agent. Thermal fluctuation spectroscopy provides a means of characterizing these different effects, potentially in a clinical milieu.

INTRODUCTION

During its lifetime of ~120 days, the red blood cell (RBC) is exposed to continuous oxidative stress. It is particularly susceptible to oxidative damage due to the high content of unsaturated fatty acid chains in the lipid bilayer (1) combined with high oxygen levels, as well as protein susceptibility to (and, as in the case of hemoglobin (Hb), promotion of) oxidative processes. Several antioxidant defense mechanisms have been identified, including removal of superoxide radicals, acceleration of the decomposition of hydrogen peroxide, and scavenging of hydroxyl radicals. Oxidative damage is also a problem in blood stored for transfusion (2,3), although the details of the mechanisms are unclear.

Oxidative damage is associated with the initial oxidation of Hb which leads to the formation of methemoglobin (MetHb), reversible hemichromes (rHCRs), and irreversible hemichromes (iHCRs) (4,5). Oxidatively denatured hemoglobin forms complexes with spectrin, thus affecting spectrin network organization and causing band 3 clustering (6–9). Hb and MetHB stabilize isolated membrane skeletons by promoting the self-association of spectrin dimers into tetramers, but further oxidation to rHCRs reverses this effect (5). The heme iron of the spectrin-bound hemoglobin catalyzes intermolecular covalent bonding through generation of hydroxyl radicals from H_2O_2 (10) forming cross-linked hemoglobin-spectrin complexes, whereas iHCRs destabilize the membrane by decreasing the formation of the spectrin-protein 4.1-actin complex (5). Oxidation of spectrin with diamide modifies the sulfhydryl groups, which results in a reduced ability of spectrin to bind to protein 4.1 and structurally causes the spectrin to acquire a circular conformation (11). Either of these changes, which may result in failure of the red cell membrane skeleton, require oxidation of only one or two sulfhydryl groups in spectrin (11) and are associated with vesiculation, apparently arising from detachment of spectrin from the membrane (12). Characteristic features of RBC aging in vivo include progressive loss of cell area and cell dehydration (13), as well as formation of Hb-spectrin complexes driven by an oxidative mechanism (14).

Hb denaturation and changes in its interactions with spectrin also influence the mobility and aggregation of band 3, the latter constituting the antigenic determinate for recognition of senescent cells (7,10). Lipid peroxidation also takes place in the membrane bilayer. It can result in extensive damage that affects membrane fluidity, membrane potential, permeability to ions, and eventual cell hemolysis; it may also cause substantial damage to membrane proteins (15).

It is clear that oxidative stress can inflict wide-ranging damage to the main structural components of the RBC responsible for the integrity and mechanical properties of the cell and can thereby impede passage of the cells through the microcirculation. Such changes may contribute to the microvascular complications that are ubiquitous in conditions, such as diabetes, that are characterized by elevated oxidative stress. The ability of the RBC to assume a parachutelike shape in small capillaries is critically dependent on its bending and shear moduli and has long been recognized as a key feature of microcirculatory hemodynamics. More recently, mechanical deformation has been shown to release ATP (16,17), and this potentially important regulator of vascular tone (18) could also be compromised by oxidation-related changes in membrane mechanics.

Submitted May 11, 2011, and accepted for publication August 31, 2011.
John P. Hale's present address is Red Cell Physiology Laboratory, New York Blood Center, New York, NY.

*Correspondence: p.g.petrov@exeter.ac.uk

Editor: Betty J. Gaffney.

0006-3495/11/10/1921/9 $2.00

doi: 10.1016/j.bpj.2011.08.053

Several studies have investigated membrane modifications due to oxidation and related changes in membrane rigidity (6,9,19,20). Typically, RBC rigidity is quantified through the changes of cell deformability as measured by, e.g., ektacytometry (6). Treatment with increasing concentrations of H_2O_2 (45–180 μM) resulted in increased membrane rigidity, appearance of echinocytes, and alternations in the lateral organization of membrane phospholipids (even though the transbilayer lipid distribution remained largely unaffected) (9). Although some lipid peroxidation was also observed, it was shown that the major changes in membrane rigidity were primarily due to formation of spectrin-globin complexes (9). A limitation of ektacytometry is that it registers only the integral response of the membrane to imposed strain. Detailed studies of the effect of oxidation on the mechanical properties of each membrane structural component, and in terms of the relevant elastic constants (bending modulus, shear modulus, and elastic interactions between the lipid bilayer and membrane skeleton) have not been undertaken. That is the aim of the study presented here. We use a detailed analysis of the membrane thermal fluctuation spectrum (21–24) to extract quantitative information about changes in the relevant membrane elastic constants of RBC membranes subjected to oxidative stress in vitro. We demonstrate that different oxidative agents can damage membrane structural components to different degrees and quantify the increased membrane rigidity in terms of bending and shear elastic moduli, as well as increased membrane tension and confining potential. Our analysis of the response of single cells to oxidative shock, without averaging over a large ensemble, also allows natural variations between the cells to be investigated.

EXPERIMENTAL SECTION

Materials and sample preparation

Fresh blood samples were collected from a healthy volunteer by pin-prick lancet (Accu-Chek Softclix Plus, Roche, Burgess Hill, UK) immediately before each experiment. A small volume, ~5 μl, was suspended in 1 ml of phosphate-buffered saline (PBS) (Oxoid, Basingstoke, UK) with 1 mg/ml bovine serum albumin (Sigma-Aldrich, Gillingham, UK). This simple buffer preserves the cell shape while minimizing solute interaction with the cell membrane, which is an important consideration for the measurement of the membrane mechanical properties. The buffer was adjusted to pH 7.4 and had an osmolarity of 290 mOsm (determined using an Osmomat 030 cryoscopic osmometer (Gonotec, Berlin, Germany)), ensuring that the cells maintained their discoid shape.

Suspended cells were placed in an open-sided observation chamber constructed from a thoroughly cleaned microscope slide and a coverslip separated by two strips of Parafilm (Pechiney Plastic Packaging, Chicago, IL) along the long edges of the slide. The Parafilm strips bond the two glass windows of the chamber together by heating briefly on a hot plate forming a chamber ~1 mm in depth. The blood suspension is introduced into the open sides of the observation chamber using a plastic pipette and is filled spontaneously under the action of the capillary forces. The slight difference between the densities of the RBCs and the surrounding PBS ensures that the cells settle on the bottom of the chamber and can conveniently be imaged using phase-contrast microscopy (see below). The average number of cells visible in the microscope field of view can be controlled by the initial dilution of the blood sample. The chamber construction allows for the exchange of buffer solution with a solution containing hydroperoxides by placing excess solution on one of the open sides of the chamber and drawing it through the chamber by means of a clean tissue of filter paper introduced at the opposite open side. During the exchange process, most of the cells do not move due to the weak adhesion to the microscope slide. To ensure full and uniform exchange of the solution, ~2 ml of peroxide solution was slowly flushed through the chamber. This procedure took ~5 min.

We induced oxidative stress in vitro using two different hydroperoxides. Hydrogen peroxide (H_2O_2) (Sigma-Aldrich) was used as a water-soluble oxidant that permeates the cell membrane and enters the cytoplasm. The second compound used was cumene hydroperoxide (cumOOH) (Sigma-Aldrich), which is expected to partition predominantly into the bilayer lipid membrane due to its hydrophobicity (25). To compare the activity of the two oxidants, both were used in bulk concentrations of 100 μM. Solutions of 100 μM H_2O_2 in PBS were prepared from fresh stock solution (0.2 M) immediately before each experiment to minimize peroxide degradation. To disperse cumOOH at the necessary concentration into PBS, the mixture was first vigorously shaken and then sonicated in an ultrasonic bath for a few minutes. It should be noted that despite all precautions taken to ensure the same peroxide concentration in all experiments, the results in different experiments were quantitatively slightly different, probably due to the peroxide decomposition and the degree of dispersion of cumOOH in PBS. To avoid possible discrepancies arising from these factors, we analyzed the thermal fluctuations of individual cells recorded during the same experiment (for each of the two peroxides), which ensured that all cells in an experiment were subjected to the same peroxide concentration.

In all experiments, cell membrane fluctuations were initially recorded while in normal PBS after the cells had stabilized on the bottom of the chamber. The buffer was then exchanged with a buffer containing either 100 μM H_2O_2 or 100 μM cumOOH (the addition of peroxide did not change the buffer osmolarity appreciably and the cells retained their biconcave shape). After the buffer was fully exchanged, RBC fluctuations were recorded at regular time intervals (typically 10 or 20 min) for a period of up to 90 min. No significant changes in the cell biconcave shape were observed, although subtle alterations (especially in the case of cells treated with cumOOH, where there was evidence of changes in the membrane area) cannot be ruled out. However, these would have been insufficient to influence the fluctuation spectra significantly.

Video microscopy and thermal fluctuation detection

To visualize the cell membrane fluctuations, we used a fast-video phase-contrast microscopy system based on a DMLFS upright microscope (Leica Microsystems GmbH, Wetzlar, Germany) equipped with a 63× PL FLUOTAR phase-contrast objective (24). Video sequences of the fluctuating red cell are recorded using a Moticam 2000 2 MP progressive scan digital video camera (Motic, Hong Kong) at a typical frame rate of 60 fps. Each frame is analyzed to determine a 2D equatorial contour to a subpixel resolution (see Supporting Material for details). Once a series of contours (between 1500 and 2500) is acquired, they are analyzed to quantify the membrane fluctuations. Each contour in the series is represented by a Fourier series (26,27) using polar coordinates (r, θ) with origin at the center of the area,

$$r(\theta) = R\left\{1 + \sum_n [a_n \cos(n\theta) + b_n \sin(n\theta)]\right\}. \quad (1)$$

The contour shape fluctuations *around the mean shape* (28) in a series are characterized by the quantity $\langle \delta_n^2 \rangle = [\langle a_n^2 \rangle - \langle a_n \rangle^2] + [\langle b_n^2 \rangle - \langle b_n \rangle^2]$ (see Supporting Material for details). The dependence of $\langle {\delta_n}^2 \rangle$ on mode number n (i.e., the contour fluctuation spectrum) is our primary experimental

measurable, to which the theoretical spectrum is fitted. We found that modes up to $n \approx 18$ can be recorded reliably using this method (higher, short-wavelength modes are affected by the optical resolution and camera noise).

The overall degree of contour fluctuations can also be quantified by analyzing the fluctuations of the radial positions, $r(\theta)/\langle r(\theta)\rangle$, of a number of chosen points (we use 360 points at positions $r(\theta)$ around the contour), as described in the Supporting Material. This analysis does not provide additional information, but it is a very sensitive measure of the overall fluctuations and can serve to monitor changes in the membrane elasticity in time.

Theoretical analysis of RBC membrane thermal fluctuations

The RBC membrane is a composite structure consisting of two essential structural components, lipid bilayer and spectrin network, which endow the membrane with its unique mechanical properties. To a first approximation, the lipid bilayer with its membrane proteins sets the bending elastic properties, since the lipid-bilayer bending modulus is substantially higher than that of the spectrin skeleton. The underlying membrane skeleton (formed by conjugated spectrin tetramers) forms a protein mesh that is sparsely attached to the bilayer, ensuring that the whole membrane possesses finite shear rigidity. To analyze our experimental contour fluctuation spectra, we use the theoretical framework developed by Safran's group (29,30). Gov et al. (29) used a free-energy functional including elastic contrubutions from the lipid bilayer, membrane skeleton, and bilayer-skeleton interactions that led to the membrane fluctuation spectrum (in the flat membrane approximation):

$$\left\langle \left| \tilde{u}(\mathbf{q}) \right|^2 \right\rangle = \frac{k_B T}{\kappa q^4 + \sigma q^2 + \gamma}, \tag{2}$$

where $\mathbf{q} = (q_x, q_y)$ is the wave vector, κ is the bilayer bending modulus, σ is the effective surface tension, γ is the strength of the confinement potential, and the other symbols have their usual meanings. Within this approach, the surface tension, σ, arises due to the attachment of the skeleton to the lipid bilayer; thus, its value is expected to be higher than the surface tension due solely to area conservation (as in skeletonless lipid vesicles). The effect of the membrane skeleton is modeled by a harmonic potential of strength γ. This is a rough, coarse-grained approximation of the effect of the skeleton that treats it as an infinitely rigid wall separated from the bilayer without explicitly taking into account the presence of the anchor sites between the protein skeleton and the lipid bilayer (29). This term in Eq. 2 results in the suppression of the long-wavelength fluctuations (see below).

In our experiments, we monitor the fluctuations of a single line in the plane of the cell equator only, i.e., we obtain the equatorial contour fluctuation spectrum. This must be accounted for when using Eq. 2 and we adapt the procedure of Pécréaux et al. (27) for lipid bilayer vesicles. First, Eq. 2 is transformed back to real space with respect to one of the spatial coordinates (e.g., y) whose value is then fixed to obtain $\langle|\tilde{u}(q_x, y = 0)|^2\rangle$, which corresponds to the experimental situation of a fluctuating line. Then, this expression is reconciled with the contour representation (Eq. 1), as described in detail in Pécréaux et al. (27). The result is

$$\left\langle c_n^2 \right\rangle = \frac{1}{2\pi} \frac{1}{\tilde{\kappa}\sqrt{\tilde{\sigma}^2 - \tilde{\gamma}}} \left[\left(\tilde{\sigma} + n^2 - \sqrt{\tilde{\sigma}^2 - \tilde{\gamma}} \right)^{-1/2} - \left(\tilde{\sigma} + n^2 + \sqrt{\tilde{\sigma}^2 - \tilde{\gamma}} \right)^{-1/2} \right], \tag{3}$$

where $\tilde{\kappa} \equiv \kappa/(k_B T)$, $\tilde{\sigma} \equiv \sigma\langle R\rangle^2/(2\kappa)$, $\tilde{\gamma} \equiv \gamma\langle R\rangle^4/\kappa$, and $n = q_x\langle R\rangle$ are dimensionless quantities and $\langle c_n^2\rangle = \langle a_n^2\rangle + \langle b_n^2\rangle$. For the case of a lipid bilayer without cytoskeleton, for which $\gamma = 0$ (and the surface tension, σ, arises only due to the area constraint), Eq. 3 reduces to the well-known equation for contour fluctuations in vesicles (cf. Eq. 15 in Pécréaux et al. (27)),

$$\left\langle c_n^2 \right\rangle = \frac{1}{2\pi} \frac{1}{\tilde{\kappa}\tilde{\sigma}} \left[\frac{1}{n} - \left(2\tilde{\sigma} + n^2 \right)^{-1/2} \right]. \tag{4}$$

We use Eq. 3 to analyze the contour fluctuation spectra ($\langle {\delta_n}^2\rangle$ vs. n) and extract values for the bending modulus, κ, membrane surface tension, σ, and strength of the confinement potential, γ, using nonlinear regression analysis. Each of these three parameters has a characteristic effect on the contour fluctuation spectrum, as illustrated in Fig. 1. Increase in the membrane bending rigidity (Fig. 1 *a*) leads to the overall shift of the whole spectrum to lower values, whereas confinement and surface tension affect predominantly the lower, longer-wavelength modes (Fig. 1, *b* and *c*). The effect of the confinement potential dominates at low n, causing strong deviations and near flattening of the fluctuation spectrum (Fig. 1 *c*). Thus, a weak dependence of the mean square amplitudes on mode number for long wavelengths is a sign of confinement. All of these fingerprint effects of κ, σ, and γ are observed in our experiments (see Results).

Equation 2 received further justification in the work of Auth et al. (30), who modeled the RBC membrane as two coupled interacting membranes (a solid membrane skeleton and a liquid lipid bilayer) at a fixed average distance apart. They demonstrated that despite the composite character of the membrane, for wavelengths $\lambda > 400$ nm, RBC fluctuations are well described by modeling the membrane as a single effective membrane whose bending

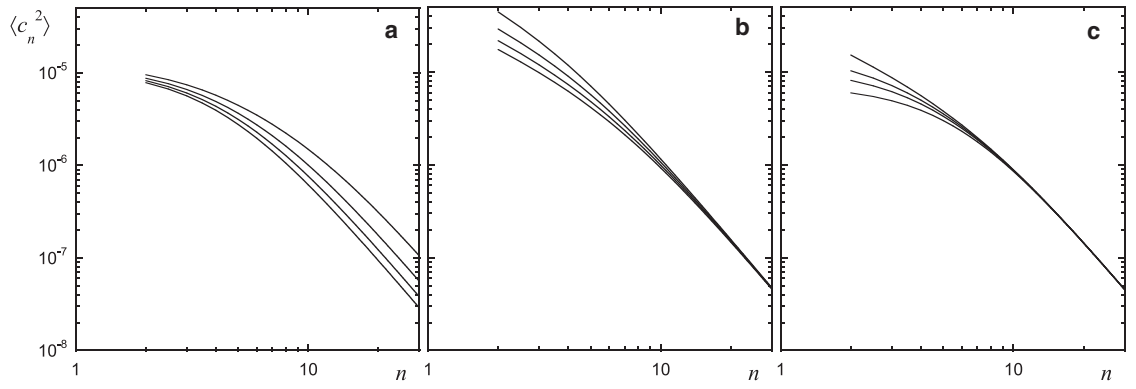

FIGURE 1 Effect of bending rigidity, surface tension, and strength of confinement on the contour fluctuation spectrum. (*a*) Effect of increasing bending rigidity: κ = (top to bottom) 2×10^{-19}, 4×10^{-19}, 6×10^{-19}, and 8×10^{-19} J ($\sigma = 2 \times 10^{-6}$ N/m, $\gamma = 9 \times 10^5$ J/m^4). (*b*) Effect of increasing surface tension: σ = (top to bottom) 5×10^{-7}, 9×10^{-7}, 1.3×10^{-6}, and 1.7×10^{-6} N/m ($\kappa = 5 \times 10^{-19}$ J, $\gamma = 0$ J/m^4). (*c*) Effect of increasing strength of confinement: γ = (top to bottom) 0, 5×10^5, 1×10^6, and 2×10^6 J/m^4 ($\kappa = 5 \times 10^{-19}$ J, $\sigma = 2 \times 10^{-6}$ N/m).

elasticity is set by the lipid bilayer. The shear modulus arising from the spectrin network, μ, results in a surface-tension-like term and a confinement potential term; these should be added to the bilayer bending term, which gives an equation for the membrane fluctuation spectrum mathematically equivalent to Eq. 2. Using a perturbative approach to account for the interaction between the bending and shear modes, Auth et al. (30) showed that the surface-tension-like term is related to the spectrin-skeleton shear modulus,

$$\sigma q^2 = \frac{9\mu k_B T}{16\pi\kappa} q^2. \quad (5)$$

The effect of confinement (due to the nonzero average curvature of the solid membrane) is also related to the spectrin-network shear modulus. The strength of the confining potential is thus given by

$$\gamma = \frac{4\mu}{A}\int_A (2H^2 - K)dA, \quad (6)$$

where A is the membrane area, H is the local mean curvature, and K is the local Gaussian curvature. Equation 5, in conjunction with Eq. 3, makes possible the evaluation of the shear elastic modulus of the spectrin skeleton from contour fluctuation spectra.

We recognize some essential limitations of this approach. Equation 2 (and, consequently, Eq. 3) is only valid in the flat-membrane limit and could legitimately be used only for fluctuations of short wavelengths compared to the cell size, $\lambda \ll R$. The lengthscale of fluctuations in our experiment, however, is comparable to the size of the cell ($\lambda \sim R$), which means that the long-wavelength fluctuation amplitudes will be affected by the overall shape of the RBC (this issue is discussed in detail in Pécréaux et al. (27) for the case of quasispherical vesicles). Since Eq. 3 does not account for the membrane geometry and assumes no difference in curvature in the plane of the contour and perpendicular to it, it will give only approximate values of the membrane elastic parameters (especially those determined from the lower modes). As evident from Fig. 1, this will affect the evaluation of the confinement potential strength and the surface tension (and, therefore, the membrane shear modulus) to a greater extent, as these quantities are extracted primarily from the lower fluctuation modes. We expect the bending modulus to be less affected by the membrane geometry, as it can be determined from the short-wavelength mean square amplitudes. However, since the overall membrane geometry of an RBC changes very little under the action of the hydroperoxides, our analysis can be used to compare relative changes in the membrane elastic parameters due to oxidation, which is the main outcome of this investigation: the elastic constants provide semiquantitative estimations but describe trends caused by the action of the oxidants.

Another limitation arises from the composition and structure of the lipid bilayer itself. The majority of the models (including those of Gov et al. (29) and Auth et al. (30)) assume a homogeneous liquid lipid bilayer characterized by a uniform bending rigidity. However, membrane proteins (and lipid domains) will modify the membrane fluctuation spectrum, as demonstrated by Reister-Gottfried et al. (31). Again, the effect is most pronounced for long wavelengths and depends on a number of factors, such as the bending rigidity of the embedded protein, as well as its spontaneous curvature, size, and surface density, some of which are difficult to determine experimentally.

The question of whether the RBC membrane fluctuations are entirely thermally driven or have a partial active component is still debated in the literature (see, e.g., (23,32–36)). Here, we treat the membrane fluctuations as thermally excited.

RESULTS AND DISCUSSION

Contour fluctuation spectra

Fig. 2 shows typical examples of the changes with incubation time of the contour fluctuation spectra of RBCs exposed to 100 μM H_2O_2 and 100 μM cumOOH. The oxidants have a considerable effect on the membrane fluctuation dynamics. Within the first 45 min, cells exposed to H_2O_2 show at first a steady decrease in the mean square fluctuation of the low modes ($n < 7$) only, whereas the higher modes remain largely unaffected (Fig. 2 *a*). The cells exposed to the same bulk concentration of cumOOH show a different trend. Again, the low modes are affected and exhibit a steady decrease in time, but this is accompanied by a reduction in the fluctuation amplitudes of the high modes beginning shortly after the cumOOH addition (Fig. 2 *c*). Qualitative comparisons with Fig. 1 suggest that the action of H_2O_2 within the first hour is mainly related to the membrane skeleton (whose elastic behavior is determined by the low, long-wavelength modes). Limited (if any) modification of the properties of the lipid bilayer is evident; changes in the bending elasticity of the bilayer begin to appear only after prolonged exposure to H_2O_2 (longer than an hour) and are much less significant compared to those produced by cumOOH. CumOOH affects the lower modes but at the same time suppresses the fluctuations in the higher modes as well. We conclude that this oxidant not only affects the membrane shear elasticity but also rigidifies the lipid bilayer with respect to its bending modulus (cf. Fig. 1 *a*) by causing oxidative damage of the lipid component.

The radial fluctuation histograms (Fig. 2, *b* and *d*) demonstrate that the overall degree of membrane thermal fluctuation is greatly reduced by both peroxides. These data can be used to quantify the overall kinetics of peroxide action by using the rate of change of the standard deviation (i.e., the square root of the variance) of the normally distributed radial displacement histograms (Fig. 3). The rate of decrease in the overall fluctuation amplitudes for cells treated with cumOOH is significantly higher than that of H_2O_2-treated cells. Another difference is evident in the early stages of the oxidative process. While H_2O_2 causes suppression of the membrane fluctuations without any delay, cumOOH fluctuation suppression is preceded by a delay of ~6 min, after which suppression occurs at a faster rate than with H_2O_2. A previous study (25) on oxidative damage by H_2O_2 and cumOOH in RBCs concluded that the kinetics of oxidation were very different. While the H_2O_2 action had fast initial kinetics, lipid oxidation by cumOOH was characterized by an initial time lag. However, the cumulative oxidative stress was much higher with cumOOH. This specificity may be reflected in the time trends shown in Fig. 3. This work further demonstrates the different modes of action of the two components on membrane constituents.

Equation 3 allows for a quantitative analysis of the changes in membrane elastic parameters. We analyzed the spectra for three cells exposed to 100 μM H_2O_2 and two cells exposed to 100 μM cumOOH. Equation 3 provides physically meaningful fits for modes between (and including) 3 and 18. An example of such a fit is given in Fig. 4. From these fits, values for κ, σ, and γ were extracted, and μ was evaluated using Eq. 5.

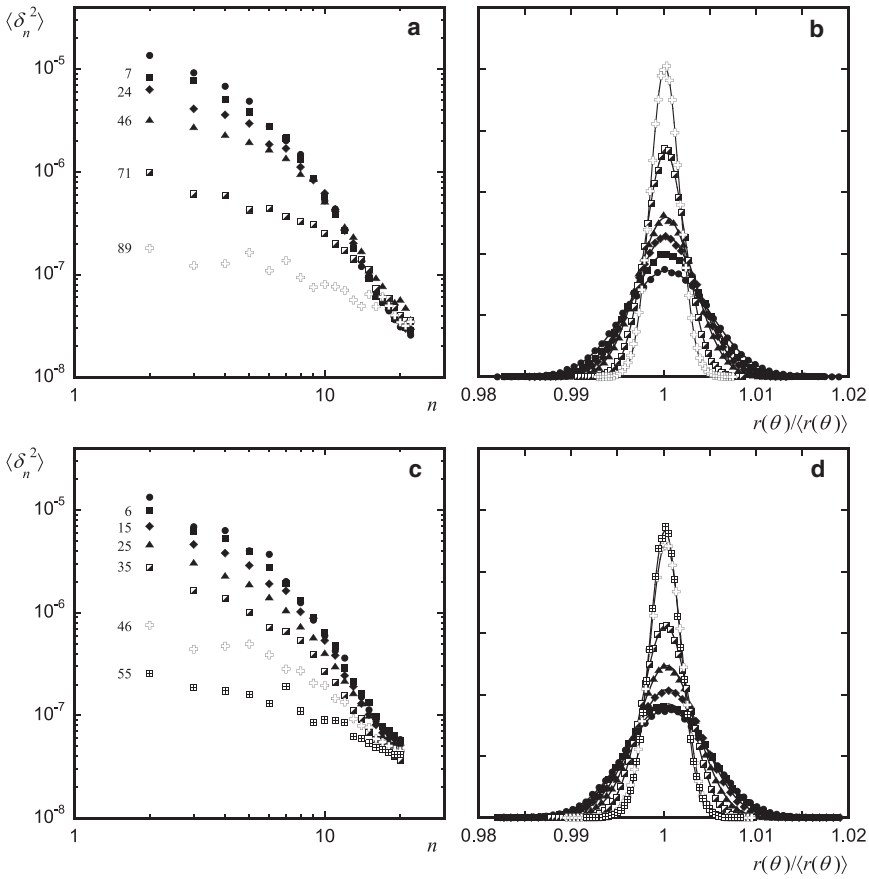

FIGURE 2 Contour fluctuation spectra (*left*) and normalized radial displacement histograms (*right*) of red cells treated with 100 μM H_2O_2 (*a* and *b*) and 100 μM comOOH (*c* and *d*) at different times of incubation. The fluctuation spectra of the untreated cells (i.e., before the infusion of the peroxide) are shown as solid circles. The other symbols indicate recordings made at times after the end of peroxide infusion, as indicated (in minutes) next to the first data points in *a* and *c*. The solid lines in *b* and *d* are fits to the normal distribution function. Symbols in *b* and *d* correspond to those in *a* and *c*.

Analysis of the untreated cells

For the five cells before treatment, we obtain an average value for the bending modulus of $\langle \kappa_0 \rangle = (5.6 \pm 0.7) \times 10^{-19}$ J. This value corresponds well to values measured previously in the same wavelength regime ($\lambda \sim R$), which range from 1.4×10^{-19} J to 4.3×10^{-19} J as measured by Peterson et al. (21), and from 2×10^{-19} J to 7×10^{-19} J as measured by Strey et al. (22). The comparison of RBC contour fluctuation spectra to coarse-grained particle dynamics simulations preformed by us previously (24) gave a similar value of 7.5×10^{-19} J. Values of this order of magnitude are typically produced in measurements at wavelengths comparable with the size of the whole cell, but studies at shorter wavelengths usually lead to bending moduli of the order of 10^{-20} J (29,37–39).

The average membrane surface tension was $\langle \sigma_0 \rangle = (1.4 \pm 0.2) \times 10^{-6}$ N/m. This value can be compared with the values obtained by Gov et al. (29) in analyzing the experimental data of Zilker et al. (37). For two RBCs they find 2.8×10^{-7} N/m and 7.7×10^{-7} N/m, not very different from ours, given the expectation that the evaluation of the surface tension from our experiment is affected by the membrane geometry (whereas the analysis in Gov et al. (29) is on lengthscales <1 μm, where the application of Eq. 2 is better justified). We also obtain a mean value of $\langle \gamma_0 \rangle = (9 \pm 3) \times 10^5$ J/m^4 for the strength of the confining potential, which is at least an order of magnitude lower than values reported by Safran's group (29,30), based on data reported for fluctuations of shorter wavelengths in discocyte RBCs. Again, this could be attributed to the different wavelength regime. However, our values of $\langle \sigma_0 \rangle$ and $\langle \gamma_0 \rangle$ are in excellent agreement with those of Daniels et al. (40), who evaluated these parameters from experiments on the growth of hemoglobin fibers confined by red cell membranes. While their value for the bending modulus, 2.0×10^{-20} J, is characteristic for the short-wavelength regime (29,37–39), the values for the membrane surface tension (1.2×10^{-6} N/m) and the strength of the confining potential (1.1×10^6 J/m^4 and 1.5×10^6 J/m^4) are very close to ours. By far, the largest discrepancy is found for the shear modulus, as obtained from Eq. 5, $\langle \mu_0 \rangle = (1.0 \pm 0.2) \times 10^{-3}$ N/m, which considerably exceeds the values typically reported in static deformation experiments, such as micropipette aspiration (6.6×10^{-6} N/m (41)), optical tweezers (2.5×10^{-6} N/m, 3.3×10^{-6} N/m (42–44)), and shear-flow experiments (1×10^{-5} N/m (45)), although values as high as 2×10^{-4} N/m have also been reported in the literature (46). Our previous analysis of contour fluctuation spectra using a coarse-grained particle dynamics simulation, which explicitly took into account the correct membrane geometry, led to a value of 3.6×10^{-6} N/m (24), entirely

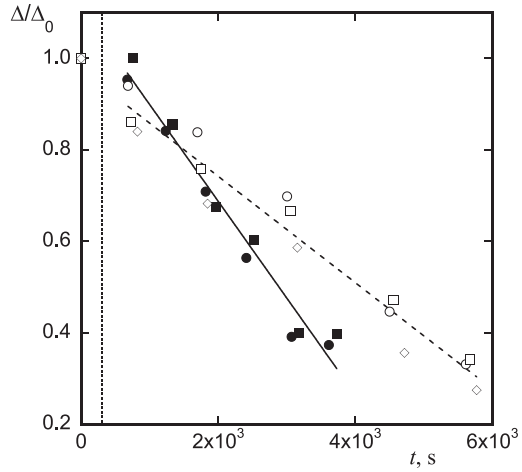

FIGURE 3 Time dependence of the standard deviation, Δ, of the normally distributed radial displacement histograms for two cells treated with cumOOH (*solid symbols*) and three cells treated with H_2O_2 (*open symbols*). The standard deviations, Δ, have been normalized with respect to those for each cell before treatment, Δ_0 (shown on the graph at time zero). The vertical dotted line (at $t = 300$ s) indicates the end of the peroxide infusion. The solid and dashed lines are guides to the eye only. The error in the determination of Δ/Δ_0 is smaller than the symbol size.

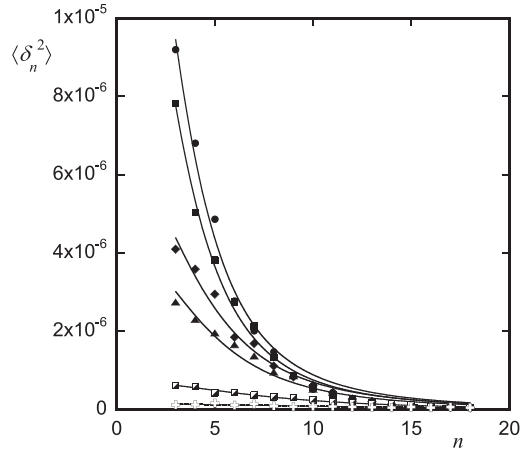

FIGURE 4 Fits of Eq. 3 (*solid lines*) to the contour fluctuation spectra obtained for a cell exposed to 100 μM H_2O_2. Modes between 3 and 18 are fitted, and values for the bending modulus, surface tension, and strength of the confining potential are extracted.

in agreement with static deformation experiments; this obviously means that the large values for μ found in this study are due to interpreting the long-wavelength modes using Eq. 3, which is derived in the flat-membrane approximation. In support of this, the values extracted by Auth et al. (30) for the shear modulus of discocyte RBCs even for short wavelengths are of the order 10^{-5} N/m or larger, the upper limit of values from static deformation experiments (45).

In addition to the limitations arising from our use of Eq. 3, there is also a systematic error in the detection of the higher modes ($n > 9$) due to the limited camera integration time (~17 ms); this results in underestimation of the real fluctuation amplitudes (see Fig. 4). We therefore present all our main findings as relative changes in membrane elastic parameters with respect to the untreated membranes.

Oxidative stress and membrane elastic properties

Fig. 5 shows the time evolution of the membrane elastic properties as a result of exposure to H_2O_2 and cumOOH. The values of the moduli are scaled to the respective values of these parameters obtained for each cell before the peroxide addition.

The change in the bending modulus of the H_2O_2-treated cells is significantly smaller than that for cumOOH-treated RBCs (Fig. 5 *a*). H_2O_2 and cumOOH are clearly distinct in their effects on the lipid bilayer elasticity. This could be understood in terms of their different solubility. H_2O_2, as a water-soluble oxidant, quickly permeates the membrane and partitions into the cytosol, where the main target for its action will be Hb (25). It will therefore have a limited effect on the membrane lipids, and the result is an approximately twofold increase of the membrane bending modulus. The fact that κ changes on a longer timescale (>1 h) may mean that some of the oxidative damage to the membrane lipids is caused by radicals formed in H_2O_2-Hb interactions, as suggested in van den Berg et al. (25). In contrast, cumOOH affects the bending modulus much more strongly, increasing its value by a factor of about 5 over that of the untreated cell. The preferential partitioning of cumOOH in the membrane will position it in immediate proximity to the membrane lipids where it is likely to initiate lipid peroxidation. Our results suggest that oxidative damage to lipids by cumOOH results in higher bending rigidity of the membrane, which is consistent with increased saturation (47) and membrane lipid packing in the plane of the membrane. A similar conclusion has been drawn in studies of lipid oxidation in unsaturated artificial bilayer membranes, which led to a decrease in membrane fluidity (48,49). This conclusion is also supported by the observation of the effects of H_2O_2 and cumOOH on the normalized mean contour radii, $\langle R\rangle/\langle R_0\rangle$ (Fig. 6). While the H_2O_2-treated cells show a small and nonsystematic change in their mean equatorial contour radius, cumOOH-treated cells, after a short lag period, show a systematic decrease in $\langle R\rangle/\langle R_0\rangle$, which is suggestive of area loss. The fact that only the membrane-soluble oxidant causes this effect is consistent with a loss in membrane area through increase in lipid packing rather than oxidation-driven loss of lipid via microvesiculation (12). The changes in the membrane bending modulus agree well with results from biochemical studies. A detailed study of the effect of these two oxidants on the kinetics and specificity of oxidative damage (25) showed that H_2O_2 (in concentrations similar to the ones used in this study), being permeable through the membrane, causes only partial lipid

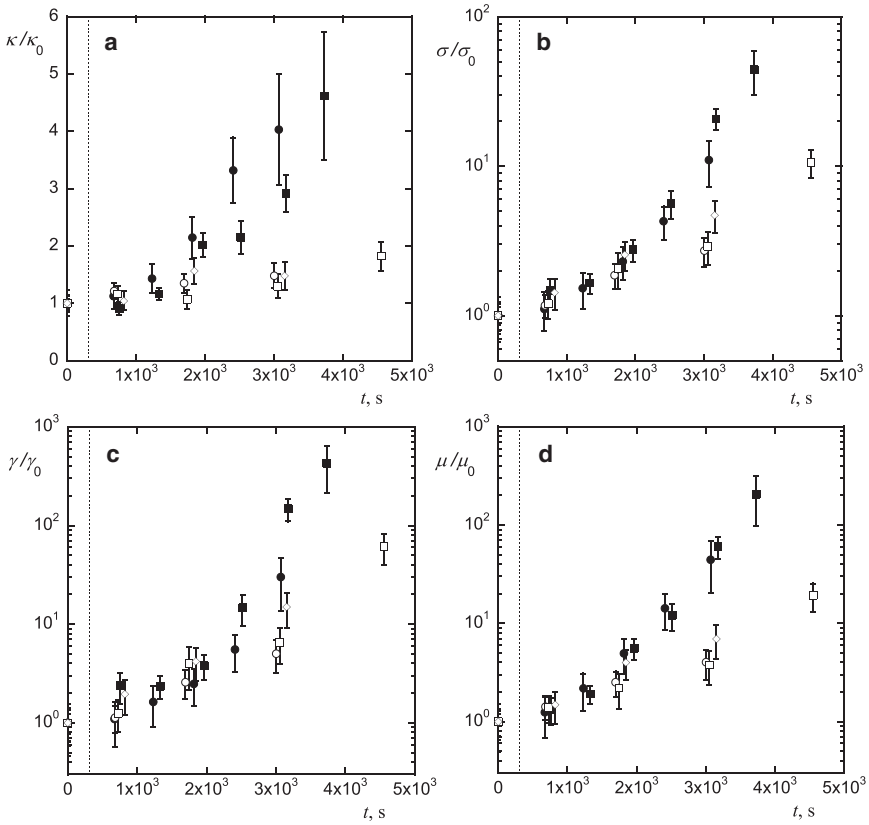

FIGURE 5 Time dependence of the relative bending modulus, κ/κ_0, membrane surface tension, σ/σ_0, strength of the confining potential, γ/γ_0, and membrane shear modulus, μ/μ_0 for two cells exposed to cumOOH (*solid symbols*) and three cells exposed to H_2O_2 (*open symbols*). The vertical dotted lines (at $t = 300$ s) indicate the end of the peroxide infusion. Note the linear scale in *a* and the semilogarithmic scales in *b–d*.

peroxidation in RBCs. Limited lipid peroxidation by H_2O_2, becoming detectable at H_2O_2 concentrations of ~135 μM, has also been reported by Snyder et al. (9). We see this effect in the twofold increase in κ. CumOOH, in contrast, led to full oxidation of the fluorescent peroxidation probe (parinaric acid) used by van den Berg and co-workers (25), indicating extensive lipid peroxidation. This is consistent with the big increase in κ (Fig. 5 *a*, *solid symbols*) and the apparent loss of membrane area suggested by the results in Fig. 6.

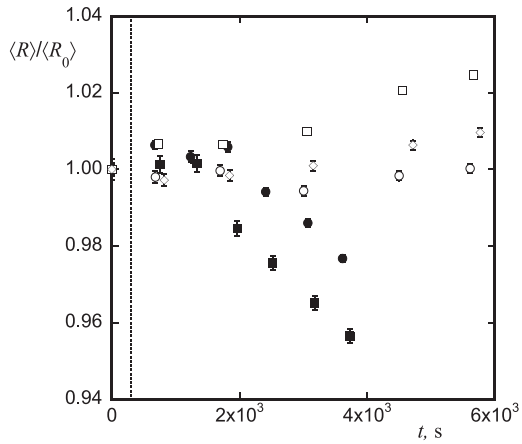

FIGURE 6 Time dependence of the normalized contour radii for two cells treated with cumOOH (*solid symbols*) and three cells exposed to H_2O_2 (*open symbols*). The vertical dotted lines (at $t = 300$ s) indicate the end of the peroxide infusion.

Fig. 5 also shows an increase in the membrane surface tension and confinement potential strength ((Fig. 5 *b* and *c*, respectively), with a concomitant rise in the membrane shear modulus (Fig. 5 *d*). The effect of cumOOH is larger than that of H_2O_2 at the same total concentrations. The shear moduli of H_2O_2-treated cells increase ~20-fold, whereas cumOOH-treated cells rigidify ~200 times (in a shorter period of time). This difference in efficiency between the two oxidants may be due to factors such as differences in oxidative end-product, differences in potency of oxidation, and/or differences in local oxidant concentration. The underlying cause for the increase in the membrane rigidity (Fig. 5 *d*) appears to be the oxidative modification of the protein component. Previous ektacytometry studies of the effect of H_2O_2 on red cell deformability (9) concluded that the main contribution to the increased membrane rigidity comes from the oxidation-induced cross-linking between Hb and spectrin (14), not from lipid peroxidation. Our results support this conclusion: H_2O_2-driven oxidative action leads to an increase in the shear rigidity (associated with the membrane protein skeleton), with only a weak effect on the bending elasticity of the lipid bilayer (Fig. 5 *a*). CumOOH, on the other hand, induces a wider spectrum of changes to the membrane mechanical properties. It shows a shear stiffening of the RBC membrane (Fig. 5 *d*) similar (albeit stronger) to

that driven by H_2O_2, most probably due to spectrin-globin complex formation, but in addition, it increases the membrane bending rigidity (Fig. 5 *a*) through oxidative damage of the membrane lipids. It is clear that different oxidants could adversely affect the mechanical properties of the membrane depending on their sites of action, their targets for oxidative damage, their potency as oxidants and the resulting end-products, and their interactions with the membrane structural components.

Finally, we note that oxidative stress may also affect the molecular- and mesoscopic-scale lateral lipid organization. Snyder et al. (9) have demonstrated that treatment of RBCs with H_2O_2 has an effect on the lateral organization of membrane lipids even though the transbilayer lipid distribution remains unaffected. They concluded that the H_2O_2-induced changes in lipid packing were due to altered membrane protein-lipid interactions. Such modifications are potentially very important, since the membrane lipid microdomain (raft) structure has been linked to membrane function in RBCs (50). Our results suggest that an even greater and more diverse impact may be expected from cumOOH-driven oxidation, which modifies significantly the protein-lipid interactions (probably in a way similar to that of H_2O_2) and also alters directly the state and packing of membrane lipids. Further experimental work is needed to clarify the effect of oxidative stress on lipid order, packing, and mesoscopic organization in erythrocyte membranes.

CONCLUSIONS

Although under normal circumstances the rate of hydrogen peroxide production in human and bovine blood plasma is of the order of μM/l/h (51,52) (with the steady-state concentration possibly much lower (51)), many abnormal conditions are related to elevated levels of oxidative species for extended periods of time. In our experiments, the red cells were exposed to high concentrations of oxidants to evaluate gross effects due to oxidative stress, but the results may be indicative of cumulative changes occurring in vivo under pathological conditions.

One of the most physiologically significant observations was the different effects of the two oxidants. In the low-mode-number regime dominated by the membrane shear modulus, both oxidants increase the value of μ. Since this parameter is related to the rigidity of the membrane protein skeleton, these observations can be explained through oxidative modifications of the membrane protein component. The main cause of rigidifying the membrane is most probably oxidatively driven spectrin-globin complex formation. In the high-mode-number regime dominated by the membrane bending rigidity (primarily a property of the lipid bilayer) only cumene hydroperoxide has a significant effect. While hydrogen peroxide has a limited oxidative effect on the membrane lipids due to its low solubility in the membrane, cumene hydroperoxide causes significant lipid peroxidation due its membrane solubility. In this case, the oxidative action is accompanied by an apparent loss of membrane area, which is indirect evidence of lipid peroxidation.

The kinetics of the overall fluctuation damping reveals that cumene hydroperoxide increases the rigidity of the membrane faster than hydrogen peroxide at equal total concentrations. This may be due to differences in the oxidative potency, differences in the end products of oxidation and their interactions with the membrane, and/or differences in the local oxidant concentrations.

The good reproducibility of the results suggests that fluctuation spectroscopy can provide a reliable means to quantitatively assess the adverse effects of reactive oxygen species on the red blood cell and distinguish differences in their effects on the lipid bilayer and the membrane skeleton. It could also provide a method of assessing the antioxidant properties of therapeutic agents.

SUPPORTING MATERIAL

Two sections (Contour Detection and Mean Contour Shapes), plus two figures and three references are available at http://www.biophysj.org/biophysj/supplemental/S0006-3495(11)01066-6.

We enjoyed fruitful discussions with W. Gratzer, J. Sleep, N. Mohandas, and P. Eggleton.

REFERENCES

1. Clemens, M. R., and H. D. Waller. 1987. Lipid peroxidation in erythrocytes. *Chem. Phys. Lipids.* 45:251–268.
2. Valtis, D. J., and A. C. Kennedy. 1954. Defective gas-transport function of stored red blood-cells. *Lancet.* 266:119–124.
3. Tinmouth, A., D. Fergusson, …, P. C. Hébert; ABLE Investigators; Canadian Critical Care Trials Group. 2006. Clinical consequences of red cell storage in the critically ill. *Transfusion.* 46:2014–2027.
4. Winterbourn, C. C. 1985. Free-radical production and oxidative reactions of hemoglobin. *Environ. Health Perspect.* 64:321–330.
5. Jarolim, P., M. Lahav, …, J. Palek. 1990. Effect of hemoglobin oxidation products on the stability of red cell membrane skeletons and the associations of skeletal proteins: correlation with a release of hemin. *Blood.* 76:2125–2131.
6. Fortier, N., L. M. Snyder, …, N. Mohandas. 1988. The relationship between in vivo generated hemoglobin skeletal protein complex and increased red cell membrane rigidity. *Blood.* 71:1427–1431.
7. Low, P. S., S. M. Waugh, …, D. Drenckhahn. 1985. The role of hemoglobin denaturation and band 3 clustering in red blood cell aging. *Science.* 227:531–533.
8. McPherson, R. A., W. H. Sawyer, and L. Tilley. 1992. Rotational diffusion of the erythrocyte integral membrane protein band 3: effect of hemichrome binding. *Biochemistry.* 31:512–518.
9. Snyder, L. M., N. L. Fortier, …, N. Mohandas. 1985. Effect of hydrogen peroxide exposure on normal human erythrocyte deformability, morphology, surface characteristics, and spectrin-hemoglobin cross-linking. *J. Clin. Invest.* 76:1971–1977.
10. Kiefer, C. R., J. F. Trainor, …, L. M. Snyder. 1995. Hemoglobin-spectrin complexes: interference with spectrin tetramer assembly as a

mechanism for compartmentalization of band 1 and band 2 complexes. *Blood.* 86:366–371.

11. Becker, P. S., C. M. Cohen, and S. E. Lux. 1986. The effect of mild diamide oxidation on the structure and function of human erythrocyte spectrin. *J. Biol. Chem.* 261:4620–4628.
12. Wagner, G. M., D. T.-Y. Chiu, …, B. H. Lubin. 1987. Spectrin oxidation correlates with membrane vesiculation in stored RBCs. *Blood.* 69:1777–1781.
13. Waugh, R. E., M. Narla, …, G. L. Dale. 1992. Rheologic properties of senescent erythrocytes: loss of surface area and volume with red blood cell age. *Blood.* 79:1351–1358.
14. Sauberman, N., N. L. Fortier, …, L. M. Snyder. 1983. Spectrin-haemoglobin crosslinkages associated with in vitro oxidant hypersensitivity in pathologic and artificially dehydrated red cells. *Br. J. Haematol.* 54:15–28.
15. Gutteridge, J. M. 1995. Lipid peroxidation and antioxidants as biomarkers of tissue damage. *Clin. Chem.* 41:1819–1828.
16. Sprague, R. S., M. L. Ellsworth, …, A. J. Lonigro. 1998. Deformation-induced ATP release from red blood cells requires CFTR activity. *Am. J. Physiol.* 275:H1726–H1732.
17. Sprague, R. S., A. H. Stephenson, …, A. J. Lonigro. 2006. Reduced expression of $G(_i)$ in erythrocytes of humans with type 2 diabetes is associated with impairment of both cAMP generation and ATP release. *Diabetes.* 55:3588–3593.
18. Ellsworth, M. L., C. G. Ellis, …, R. S. Sprague. 2009. Erythrocytes: oxygen sensors and modulators of vascular tone. *Physiology (Bethesda).* 24:107–116.
19. Hebbel, R. P., A. Leung, and N. Mohandas. 1990. Oxidation-induced changes in microrheologic properties of the red blood cell membrane. *Blood.* 76:1015–1020.
20. Schrier, S. L., and N. Mohandas. 1992. Globin-chain specificity of oxidation-induced changes in red blood cell membrane properties. *Blood.* 79:1586–1592.
21. Peterson, M. A., H. Strey, and E. Sackmann. 1992. Theoretical and phase contrast microscopic eigenmode analysis of erythrocyte flicker: amplitudes. *J. Phys. II France.* 2:1273–1285.
22. Strey, H., M. Peterson, and E. Sackmann. 1995. Measurement of erythrocyte membrane elasticity by flicker eigenmode decomposition. *Biophys. J.* 69:478–488.
23. Evans, J., W. Gratzer, …, J. Sleep. 2008. Fluctuations of the red blood cell membrane: relation to mechanical properties and lack of ATP dependence. *Biophys. J.* 94:4134–4144.
24. Hale, J. P., G. Marcelli, …, P. G. Petrov. 2009. Red blood cell thermal fluctuations: comparison between experiment and molecular dynamics simulations. *Soft Matter.* 5:3603–3606.
25. van den Berg, J. J. M., J. A. Op den Kamp, …, F. A. Kuypers. 1992. Kinetics and site specificity of hydroperoxide-induced oxidative damage in red blood cells. *Free Radic. Biol. Med.* 12:487–498.
26. Döbereiner, H.-G., G. Gompper, …, K. A. Riske. 2003. Advanced flicker spectroscopy of fluid membranes. *Phys. Rev. Lett.* 91:048301.
27. Pécréaux, J., H.-G. Döbereiner, …, P. Bassereau. 2004. Refined contour analysis of giant unilamellar vesicles. *Eur. Phys. J. E Soft Matter.* 13:277–290.
28. Duwe, H. P., J. Kaes, and E. Sackmann. 1990. Bending elastic moduli of lipid bilayers: modulation by solutes. *J. Phys. France.* 51:945–962.
29. Gov, N., A. G. Zilman, and S. Safran. 2003. Cytoskeleton confinement and tension of red blood cell membranes. *Phys. Rev. Lett.* 90:228101.
30. Auth, T., S. A. Safran, and N. S. Gov. 2007. Fluctuations of coupled fluid and solid membranes with application to red blood cells. *Phys. Rev. E.* 76:051910.
31. Reister-Gottfried, E., S. M. Leitenberger, and U. Seifert. 2010. Diffusing proteins on a fluctuating membrane: analytical theory and simulations. *Phys. Rev. E.* 81:031903.
32. Levin, S., and R. Korenstein. 1991. Membrane fluctuations in erythrocytes are linked to MgATP-dependent dynamic assembly of the membrane skeleton. *Biophys. J.* 60:733–737.
33. Tuvia, S., A. Almagor, …, S. Yedgar. 1997. Cell membrane fluctuations are regulated by medium macroviscosity: evidence for a metabolic driving force. *Proc. Natl. Acad. Sci. USA.* 94:5045–5049.
34. Tuvia, S., S. Levin, …, R. Korenstein. 1998. Mechanical fluctuations of the membrane-skeleton are dependent on F-actin ATPase in human erythrocytes. *J. Cell Biol.* 141:1551–1561.
35. Szekely, D., T. W. Yau, and P. W. Kuchel. 2009. Human erythrocyte flickering: temperature, ATP concentration, water transport, and cell aging, plus a computer simulation. *Eur. Biophys. J.* 38:923–939.
36. Betz, T., M. Lenz, …, C. Sykes. 2009. ATP-dependent mechanics of red blood cells. *Proc. Natl. Acad. Sci. USA.* 106:15320–15325.
37. Zilker, A., H. Engelhardt, and E. Sackmann. 1987. Dynamic reflection interference contrast (RIC-) microscopy: a new method to study surface excitations of cells and to measure membrane bending elastic moduli. *J. Phys. France.* 48:2139–2151.
38. Zilker, A., M. Ziegler, and E. Sackmann. 1992. Spectral analysis of erythrocyte flickering in the 0.3–4-μM^{-1} regime by microinterferometry combined with fast image processing. *Phys. Rev. A.* 46:7998–8001.
39. Fournier, J. B., D. Lacoste, and E. Raphaël. 2004. Fluctuation spectrum of fluid membranes coupled to an elastic meshwork: jump of the effective surface tension at the mesh size. *Phys. Rev. Lett.* 92:018102.
40. Daniels, D. R., J. C. Wang, …, M. S. Turner. 2006. Deforming biological membranes: how the cytoskeleton affects a polymerizing fiber. *J. Chem. Phys.* 124:024903.
41. Waugh, R., and E. A. Evans. 1979. Thermoelasticity of red blood cell membrane. *Biophys. J.* 26:115–131.
42. Hénon, S., G. Lenormand, …, F. Gallet. 1999. A new determination of the shear modulus of the human erythrocyte membrane using optical tweezers. *Biophys. J.* 76:1145–1151.
43. Dao, M., C. T. Lim, and S. Suresh. 2003. Mechanics of the human red blood cell deformed by optical tweezers. *J. Mech. Phys. Solids.* 51:2259–2280.
44. Dao, M., C. T. Lim, and S. Suresh. 2005. Mechanics of the human red blood cell deformed by optical tweezers [Journal of the Mechanics and Physics of Solids, 51 (2003) 2259–2280]. *J. Mech. Phys. Solids.* 53:493–494.
45. Hochmuth, R. M., N. Mohandas, and P. L. Blackshear, Jr. 1973. Measurement of the elastic modulus for red cell membrane using a fluid mechanical technique. *Biophys. J.* 13:747–762.
46. Sleep, J., D. Wilson, …, W. Gratzer. 1999. Elasticity of the red cell membrane and its relation to hemolytic disorders: an optical tweezers study. *Biophys. J.* 77:3085–3095.
47. Rawicz, W., K. C. Olbrich, …, E. Evans. 2000. Effect of chain length and unsaturation on elasticity of lipid bilayers. *Biophys. J.* 79:328–339.
48. Dobretsov, G. E., T. A. Borschevskaya, …, Y. A. Vladimirov. 1977. The increase of phospholipid bilayer rigidity after lipid peroxidation. *FEBS Lett.* 84:125–128.
49. Borst, J. W., N. V. Visser, …, A. J. W. G. Visser. 2000. Oxidation of unsaturated phospholipids in membrane bilayer mixtures is accompanied by membrane fluidity changes. *Biochim. Biophys. Acta.* 1487: 61–73.
50. Salzer, U., and R. Prohaska. 2001. Stomatin, flotillin-1, and flotillin-2 are major integral proteins of erythrocyte lipid rafts. *Blood.* 97:1141–1143.
51. Giulivi, C., P. Hochstein, and K. J. A. Davies. 1994. Hydrogen peroxide production by red blood cells. *Free Radic. Biol. Med.* 16:123–129.
52. Lacy, F., M. T. Kailasam, …, R. J. Parmer. 2000. Plasma hydrogen peroxide production in human essential hypertension: role of heredity, gender, and ethnicity. *Hypertension.* 36:878–884.